

Novel Strategy for Constructing High Efficiency OLED Emitters with Excited State Quinone-Conformation Induced Planarization Process

Haozhong Wu, Yuyu Pan, Jiajie Zeng, Lili Du, Wenwen Luo, Han Zhang, Kaiqi Xue, Ping Chen, David Lee Phillips, Zhiming Wang,* Anjun Qin, and Ben Zhong Tang*

In contrast to the common intramolecular charge transfer (ICT) emission, planarized intramolecular charge transfer (PLICT) based materials usually possess higher proportion radiative decay for their flat and rigid conformation in excited states. Herein, a strategy for designing PLICT-based emitters by the excited state quinone-conformation induced planarization is proposed. By virtue of RIR mechanism on TPP (tetraphenylpyrazinyl) unit, the newcomers named as TPP-PPI (1-phenyl-2-(4'-(3,5,6-triphenylpyrazin-2-yl)-[1,1'-biphenyl]-4-yl)-1H-phenanthro[9,10-d]imidazole) and TPP-PI (1-phenyl-2-(4-(3,5,6-triphenylpyrazin-2-yl)phenyl)-1H-phenanthro[9,10-d]imidazole) exhibit aggregation-induced emission (AIE) characteristics. TPP-PPI and TPP-PI have obvious PLICT properties via series of spectral measurements. Employing theoretical calculation in ground and excited states in different solvents, their PLICT process is confirmed further, and TPP's contribution on PLICT formation becomes clear. In non-doped organic light-emitting diodes, these two emitters with AIE and PLICT characteristic exhibit good performance with external quantum efficiency (4.85% and 4.36%) as blue emitters.

charge transfer (ICT) states which depend on the electronic nature and the connecting patterns of donors (D) and acceptors (A). In most cases, the large torsion between D and A results in small overlapping of frontier orbitals and is detrimental to radiative decay process.^[5] Furthermore, the structure would be strong polarized and twisted by polar solvent, so the elevation of highest occupied molecular orbital (HOMO) level and narrowing the bandgap, generates the redshift in its photoluminescence spectrum.^[6]

For achieving strong emission of D-A molecules, some ICT materials are constructed by D- π -A mode instead of D-A type for preventing serious distortion, and their OLEDs performance would be improved obviously.^[7] Klymchenko et al. replaced naphthalene core by fluorene to extend electronic conjugation and FR0 (7-diethylamino-9,9'-dimethyl-9H-fluorene-2-carbaldehyde) still exhibits strong fluorescence and large Stokes shift in high polar solvents.^[8] Konishi et al. inhibited the distortion of biphenyl unit through bonding methylene- and ethylene-bridge on dimethylaniline-benzaldehyde derivatives.^[6]


Recently, Haberhauer et al. proposed the model of planarized intramolecular charge transfer (PLICT) states that the conformations are flatter in their excited states than these in ground

1. Introduction

Materials of π -conjugated push-pull systems have been extensively investigated in decades for excellent charge transporting ability and environment sensitivity, so they have been applied in organic light-emitting diodes (OLEDs), non-linear optical data, photovoltaic devices and chemsensors.^[1–4] The photophysical properties of these materials often affect by intramolecular

H. Wu, J. Zeng, W. Luo, H. Zhang, Prof. Z. Wang, Prof. A. Qin, Prof. B. Z. Tang
State Key Laboratory of Luminescent Materials and Devices
Center for Aggregation-Induced Emission
Guangzhou International Campus
South China University of Technology (SCUT)
Guangzhou 510640, China
E-mail: wangzhiming@scut.edu.cn; tangbenz@ust.hk

Prof. Y. Pan
School of Petrochemical Engineering
Shenyang University of Technology (SUT)
Liaoyang 111003, China

 The ORCID identification number(s) for the author(s) of this article can be found under <https://doi.org/10.1002/adom.201900283>.

K. Xue, Prof. P. Chen
State Key Laboratory on Integrated Optoelectronics
Jilin University
Changchun 130012, China

Dr. L. Du, Prof. D. L. Phillips
Department of Chemistry
The University of Hong Kong
Pokfulam Road, 999077 Hong Kong, China

Prof. Z. Wang, Prof. B. Z. Tang
HKUST-Shenzhen Research Institute
Shenzhen 518057, China

Prof. Z. Wang, Prof. B. Z. Tang
Department of Chemistry
The Hong Kong University of Science and Technology (HKUST)
Clear Water Bay, Kowloon, 999077 Hong Kong, China

DOI: 10.1002/adom.201900283

states.^[9] They employed AD–D' structure to realize their idea. In ground states, the repulsion of p electrons on nitrogen atoms lead to the distortion of the AD–D'. After excitation, the D' can compensate the electron deficiency of A–D⁺ while they are in the same plane. The planar structures can stimulate the good conjugation between donors and acceptors so result in efficient overlapping of frontier orbitals with large transition moments. Zhang *et al.* discovered the PLICT characteristic in 1,3-dioxolane derivatives and the 1,3-dioxolane group may be the key factor for PLICT formation.^[10] However, none of them employed these type materials in OLED application.

Aggregation-induced emission (AIE) compounds are often constructed with highly twisted structures and several rotors densely combining around the luminogens causes the structure distortion in ground states.^[11] Upon excitation, some of these AIE molecules tend to be flatten, which is familiar to the PLICT model. Recently, we have discovered the AIE block named tetraphenylpyrazinyl (TPP) has large torsion among the pyrazinyl center and peripheral phenyl groups in ground state, while it prefers forming the quinone conformation upon excitation, enlarges its excited conjugation for planarization, namely excited state quinone-conformation induced planarization (ESQIP).^[12] Based on these, we attempted to rely on this peculiarity of TPP to construct PLICT-based materials and applied their derivatives in OLEDs.

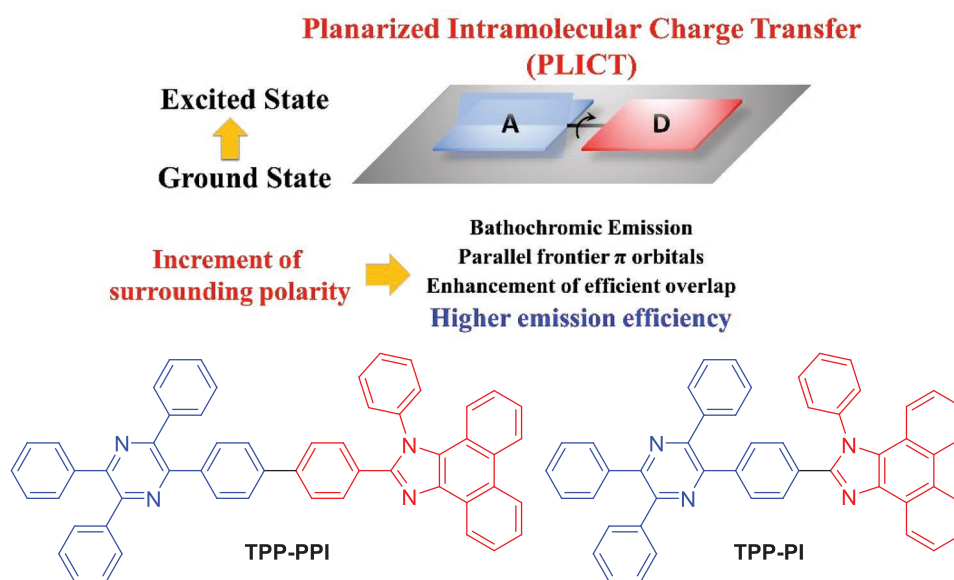
Here, we choose 1-phenyl-1H-phenanthro[9,10-d]imidazole (PI) as donor because PI is a rigid π donor and does not cause significant conformational variation upon excitation. Two blue D-A typed TPP derivatives, 1-phenyl-2-(4'-(3,5,6-triphenylpyrazin-2-yl)-[1,1'-biphenyl]-4-yl)-1H-phenanthro[9,10-d]imidazole (TPP-PPI) and 1-phenyl-2-(4'-(3,5,6-triphenylpyrazin-2-yl)phenyl)-1H-phenanthro[9,10-d]imidazole (TPP-PI) are prepared (Scheme 1). Expectably, they exhibit obvious AIE feature and strong fluorescence in polar solvents. Combining theoretical calculation in ground and excited states, the change in conformation and their tuning trend on fluorescence peak

shift and oscillator strength (*f*) are confirmed in further. In non-doped blue OLEDs, TPP-PPI and TPP-PI display good performance with high external quantum efficiency (EQE) and low roll-off. All data prove that we might develop a novel strategy for high-efficiency OLED emitters by using TPP block.

2. Results and Discussion

2.1. Synthesis and Characterization

All solvents and reagents were purchased from commercial suppliers and used without further purification. The synthetic route of the two products is outlined in Scheme S1 and some synthesis details are shown in Supporting Information. The intermediate 1 is synthesized according to the previous literatures.^[12] TPP-PPI is obtained through Suzuki coupling reaction from the intermediate 1 and imidazole ring formation reaction successively.^[13] TPP-PI is obtained from 3 via Sonogashira coupling reaction, oxidation, and reacting with 1,2-diphenylethane 1,2-diamine.^[14] TPP-PPI and TPP-PI are soluble in common organic solvents, such as tetrahydrofuran (THF), dichloromethane (DCM), and so on, but not in water. Both target products are further purified through temperature-gradient vacuum sublimation in vacuum deposition before their characterization and OLED device fabrication. The thermal properties of TPP-PPI and TPP-PI are measured by thermogravimetric analysis (TGA) and differential scanning calorimetry (DSC). Both of them exhibit good thermal stability with 5% weight loss temperature (*T*₅) of 432 and 453 °C, respectively (Figure S17, Supporting Information). Adequate glass-transition temperatures (*T*_g) of 164 and 148 °C determined for TPP-PPI and TPP-PI reveal the good morphological stability. The energy levels of HOMOs and lowest unoccupied molecular orbitals (LUMOs) are obtained by cyclic voltammetry (Figure S16, Supporting Information). The HOMOs of TPP-PPI and TPP-PI



Scheme 1. The PLICT model and molecular structure of TPP-PPI and TPP-PI.

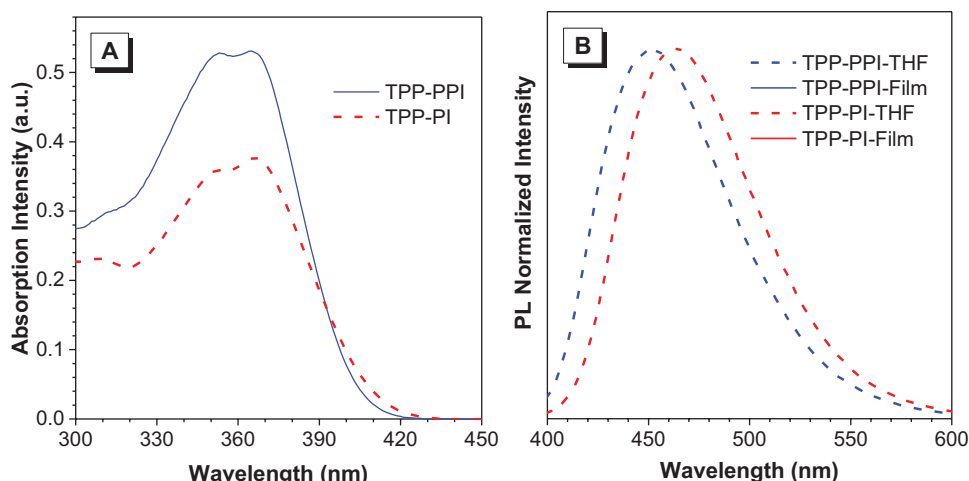


Figure 1. A) Absorption spectra in THF solutions (10×10^{-6} M) and B) PL spectra in THF solutions (10×10^{-6} M) and solid films of TPP-PPI and TPP-PI.

are estimated at -5.54 and -5.45 eV, while their LUMOs are at -2.90 and -2.85 eV, respectively. The data mentioned above for TPP-PPI and TPP-PI are summarized at Table S1 in the Supporting Information.

2.2. Photophysical Properties

The photophysical properties of the two compounds were analyzed based on the absorption spectrum and photoluminescence (PL) spectrum. As shown in **Figure 1**, they all exhibit two strong absorption band 330–400 nm in THF solution, which can be assigned to the $\pi-\pi^*$ transition of phenanthro[9,10-d]imidazole-based derivatives. TPP-PPI and TPP-PI both exhibit blue emission with the peak at 452 and 463 nm in the dilute THF solution, accompanying with fluorescence quantum yields (Φ s) of 10.0% and 13.8%, respectively. In contrast to the emission in THF solution, they generate stronger emission with the peaks at 470 and 481 nm in the neat film, and their Φ s improve to 28.1% and 20.2%, respectively, indicative of the AIE nature. Similar to most of AIEgens, their enhancing PL intensities from solution to solid still are from the synergy effect of increase of radiative decay rate (K_r) and decrease of non-radiative decay rate (K_{nr}) which are calculated from their Φ s and lifetime (τ) following the Equations (1) and (2):^[15]

$$K_r = \frac{\Phi}{\tau} \quad (1)$$

$$K_{nr} = \frac{1-\Phi}{\tau} \quad (2)$$

Table 1. The photo-physical data of TPP-PPI and TPP-PI.

	λ_{abs}^a [nm]	λ_{em}^b [nm]		Φ^c [%]		τ^d [ns]		K_r^e [10^8]		K_{nr}^f [10^8]	
		Soln	Film	Soln	Film	Soln	Film	Soln	Film	Soln	Film
TPP-PPI	365	452	470	10.0	28.1	0.51	0.82	1.96	3.43	17.65	8.77
TPP-PI	366	463	481	13.8	20.2	0.73	0.93	1.89	2.17	11.81	8.58

^a)Maximum absorption wavelength, concentration: 10×10^{-6} M; ^b)Maximum emission wavelength, soln: THF solution, film: neat film; ^c)Absolute fluorescence quantum efficiency; ^d)Fluorescence lifetime; ^e) $K_r = \Phi/\tau$; ^f) $K_{nr} = (1 - \Phi)/\tau$.

All the photophysical details of TPP-PPI and TPP-PI are summarized in **Table 1**.

To further verify their AIE activity, the emission behaviors of two compounds in nanoaggregates were investigated. Taking TPP-PPI as an example (**Figure 2**), its PL intensity remains low when the water fraction (f_w , vol %) is less than 60% in the THF/water mixture, but it increases rapidly when the f_w is more than 80%. The higher the water fraction is, the stronger the PL intensity is, which demonstrates its AIE activity. In fact, the nanoaggregate formation restricts intramolecular rotations and obstructs the non-radiative decay channel, and surely contributes to the enhanced emission.^[15] Moreover, the PL spectra redshifts from 452 to 467 nm with the increment of f_w under $f_w = 60\%$ (no aggregate formation), inferring that TPP-PPI exists ICT effect (**Figure 2A**, inset). As f_w is added to 99%, the PL intensity decreases because of the precipitate formation. Similar PL enhancements and redshift are also observed for TPP-PI (**Figure S18**, Supporting Information).

The solvatochromism of these compounds in different solvents (*n*-hexane, triethylamine, ethyl acetate, THF, DCM, and acetonitrile) was attempted. For TPP-PPI, the absorption spectrum display that its absorption profiles change little and are nearly independent on the influence of solvent polarity (**Figure S19A**, Supporting Information). Nevertheless, the apparent redshift of maximum emissive wavelength from 431 nm in *n*-hexane to 484 nm in acetonitrile are displayed (**Figure 3A** and **Table S2**, Supporting Information), and should be attributed to the ICT effect, which suggests that the dipole moment of TPP-PPI in excited state is more sensitive to solvent than that in ground state. Against to the common ICT process, TPP-PPI exhibits

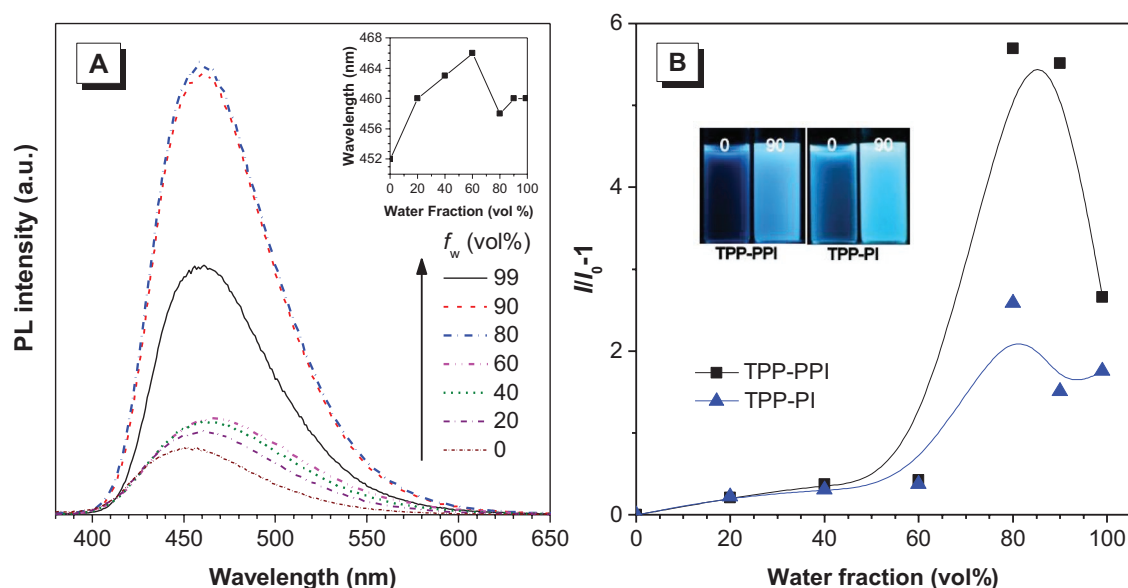


Figure 2. A) The PL spectra of TPP-PPI in THF/water mixture with different water fractions (10×10^{-6} M); Inset: changes of the maximum emissive wavelength of TPP-PPI in THF/water mixture with different water fractions. B) The changes of relative PL intensity of TPP-PPI and TPP-PI in THF/water mixture with different water fractions.

gradual increase in Φ_s with increasing solvent polarity, such as 2.7% in *n*-hexane, 10.3% in THF, and 19.7% in acetonitrile, which accords with PLICT feature. The results preliminarily verify the feasibility of strategy about utilizing TPP block to construct PLICT molecules, and the same results are also appeared in TPP-PI (Figure S20 and Table S3, Supporting Information). Besides, their absorption spectrum, PL spectrum, Φ_s , and lifetime were measured in *n*-hexane/THF/acetonitrile (CH_3CN) mixtures with different fractions. As shown in Figure 3B, and Figure S21 and Tables S4 and S5, Supporting Information, both TPP-PPI and TPP-PI exhibit gradual redshift emission and enhanced Φ_s along with the increasing of the THF fraction in *n*-hexane/THF mixture (H:T) or the CH_3CN fraction in THF/ CH_3CN mixture (T:C), respectively. Similar to the experiment in different fraction mixture solvents, there is little change in

their absorption spectra and distinct redshift in emission peaks, which indicates that the excited states dipole moment of TPP-PPI or TPP-PI is surly more sensitive to solvent polarity than theirs in ground states again.

Based on these results, the change in wavelength and Φ_s should may originate from the formation of large conjugation and rigid structure when they are excited, and the polar solvent could amplify this effect, which is in accordance with PLICT characteristic.^[9] If our speculation is correct, the K_r of TPP-PPI or TPP-PI would become larger and their K_{nr} should decrease with increasing solvent polarity, because non-radiative relaxation usually would be restricted along with their rigidity increase. The expected change trends of K_r and K_{nr} are appeared as described in Table S4 in the Supporting Information, which may demonstrates the excited states of TPP-PPI

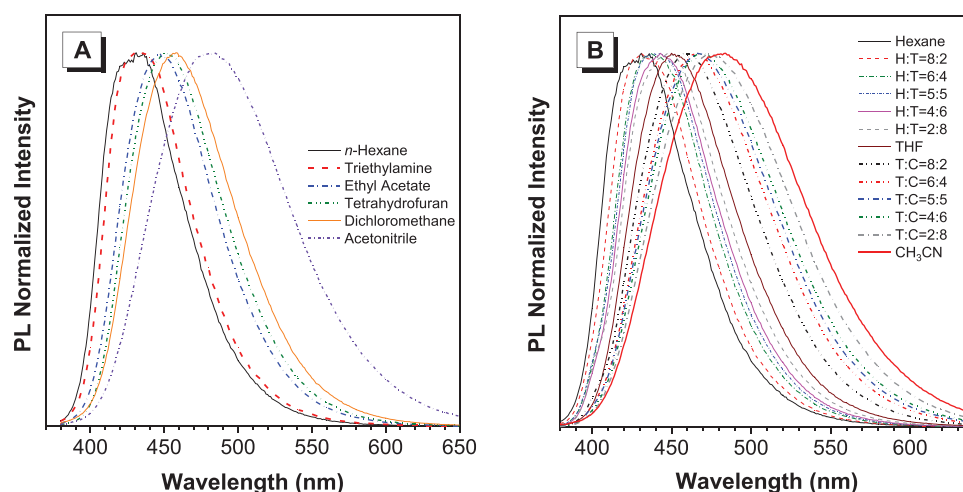


Figure 3. A) Normalized PL spectra of TPP-PPI in solvents with various polar parameters; and B) normalized PL spectra of TPP-PI in *n*-Hexane/THF/ CH_3CN mixture with different fraction (10×10^{-6} M).

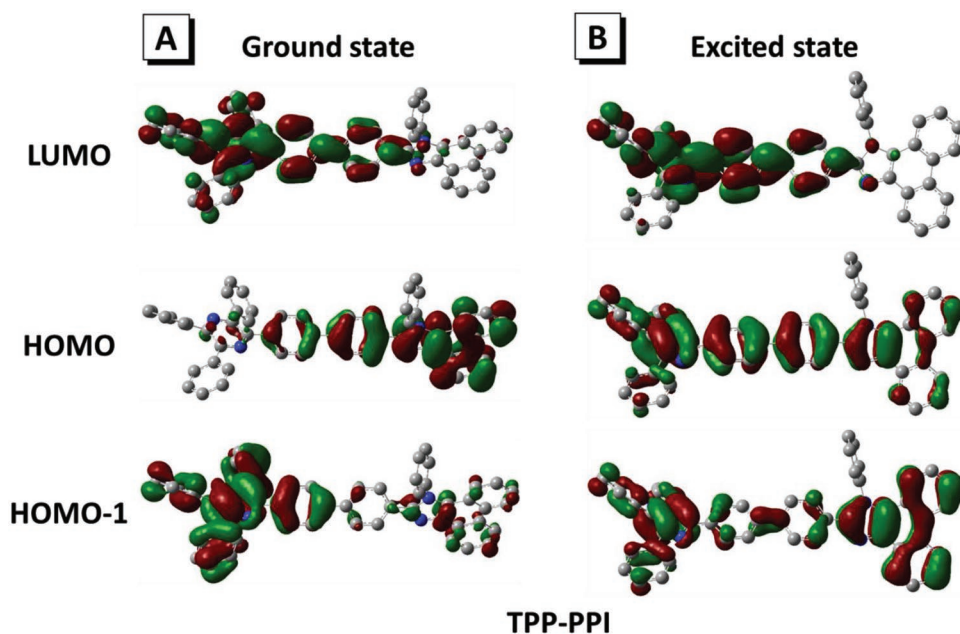


Figure 4. Frontier orbital amplitude plot of TPP-PPI in A) ground state and B) excited state.

really undergo PLICT process. The same results are confirmed in TPP-PI (Table S5, Supporting Information).

2.3. Theoretical Calculations

To interpret PLICT process of TPP-based materials, quantum-chemical calculations were performed using density functional theory (DFT) and time dependent density functional theory (TD-DFT) calculations with the M062X/6-31G(d,p) level in Polarized Continuum Model for their ground and excited states, respectively. The optimized geometries of two compounds in *n*-Hexane, THF and CH₃CN are depicted in Figure S22, Supporting Information. As expected (Figure 4 and Figure S23, Supporting Information), the HOMOs of TPP-PPI and TPP-PI mainly locate at the phenanthro[9,10-d]imidazole units, while the LUMOs are localized mostly over the tetraphenylpyrazine core in their ground states. However, the HOMO-1s and HOMOs are almost dispersed on entire molecules in their excited states. The results of the calculated photophysical data of both compounds are shown in Table 2, while the other data about the change of bond length and dihedral angle are summarized in Table 3 for TPP-PPI (Table S7, Supporting Information for TPP-PI).

As shown in Table 2, calculated emission peaks in TPP-PPI and TPP-PI exhibit bathochromic shift from *n*-hexane to CH₃CN, and the tendency is consistent with the experimental results. It demonstrates this calculation method is valid and reasonable. Emission of TPP-PPI and TPP-PI originates from transition between the HOMO and LUMO mostly and a fraction of the transition among the HOMO-1 and LUMO. As shown in Figure 4B, the transition of HOMO-1 → LUMO has more CT proportion than that of HOMO → LUMO. Generally, the increment of localized excited state (LE) proportion and oscillator strength (*f*) would be benefit to the Φ improvement. Whether TPP-PPI or TPP-PI, the fraction of transition from HOMO to

LUMO and *f* become large from the *n*-hexane to CH₃CN, which is matched to the experimental observation.

From the view of structure properties, the variety of dihedral angle (α) and bond length (*L*) are the most convincing evidence for PLICT process. As shown in Figure 5C and Table 3, $\alpha_{17-16-54-55}$, $\alpha_{56-57-18-24}$, $\alpha_{21-22-30-31}$, and $\alpha_{32-33-37-44}$ of TPP-PPI in excited states all become smaller than their ground states in three selected solvent, e.g. in *n*-hexane, the $\alpha_{17-16-54-55}$, $\alpha_{56-57-18-24}$, $\alpha_{21-22-30-31}$, and $\alpha_{32-33-37-44}$ decrease from 27.70°, 35.91°, 35.71°, and 35.58° in ground state to 19.32°, 22.30°, 12.78°, and 18.17° in excited state. It speculates that the conformation of TPP-PPI become planar in excited states. Although the pyrazine ring ($\alpha_{31-32-34-35}$) is a little twisted in excited states (7.29° in *n*-hexane, 6.72° in THF, and 6.49° in CH₃CN) comparing to its ground states (6.55° in *n*-hexane, 6.16° in THF, and 6.08° in CH₃CN), the pyrazine gives a planarization tendency along with the increment of surrounding polarity. The similar process appears in $\alpha_{21-22-30-31}$ and $\alpha_{32-33-37-44}$ of TPP-PPI, whose excited states change from 12.78° and 18.17° to 11.41° and 16.46° when *n*-hexane is replaced by CH₃CN, respectively. Additionally, the

Table 2. Theoretically calculated data in the optimized structures of TPP-PPI and TPP-PI in the *n*-hexane/THF/CH₃CN. (*E*: the energy of S₁ to S₀, *f*: the oscillator strength of S₁ to S₀, and *P*: the ratio of main electron configurations).

		<i>E</i> (eV)	λ [nm]	<i>f</i>	S ₁ → S ₀	
					<i>P</i> (H-1 → L)	<i>P</i> (H → L)
TPP-PPI	<i>n</i> -hexane	2.80	443	1.4087	0.119	0.824
	THF	2.68	463	1.4837	0.096	0.850
	CH ₃ CN	2.63	472	1.4991	0.089	0.860
TPP-PI	<i>n</i> -hexane	2.78	446	1.4055	0.050	0.898
	THF	2.66	465	1.5989	0.043	0.904
	CH ₃ CN	2.62	473	1.6568	0.042	0.906

Table 3. Selected dihedral [α] (unit: degree) and selected bond length [L] (unit: Å) in the optimized structures of TPP-PPI in the *n*-hexane/THF/CH₃CN ($\Delta = X_{\text{Excited}} - X_{\text{Ground}}$, $X = \alpha$ or L).

		$\alpha_{17-16-54-55}$	$\alpha_{56-57-18-24}$	$\alpha_{21-22-30-31}$	$\alpha_{31-32-34-35}$	$\alpha_{32-33-37-44}$	L_{16-54}	L_{18-57}	L_{22-30}	L_{31-32}	L_{34-35}	L_{33-37}
Hexane	Ground	27.70	35.91	35.71	6.55	35.58	1.474	1.482	1.485	1.333	1.332	1.486
	Excited	19.32	22.30	12.78	7.29	18.17	1.463	1.454	1.417	1.320	1.308	1.455
	Δ	-8.38	-13.61	-22.93	0.74	-17.41	-0.011	-0.028	-0.068	-0.013	-0.024	-0.031
THF	Ground	28.81	34.73	36.58	6.16	37.56	1.474	1.483	1.485	1.334	1.332	1.486
	Excited	21.39	21.48	11.85	6.72	17.00	1.465	1.454	1.413	1.318	1.307	1.452
	Δ	-7.42	-13.25	-24.73	0.56	-20.56	-0.009	-0.029	-0.072	-0.016	-0.025	-0.034
CH ₃ CN	Ground	29.21	34.13	36.69	6.08	38.16	1.474	1.483	1.485	1.334	1.333	1.486
	Excited	22.37	21.00	11.41	6.49	16.46	1.465	1.454	1.411	1.317	1.307	1.451
	Δ	-6.84	-13.13	-25.28	0.41	-21.70	-0.009	-0.029	-0.074	-0.017	-0.026	-0.035

difference between ground states and excited states of $\alpha_{21-22-30-31}$ and $\alpha_{32-33-37-44}$ are larger than that of $\alpha_{17-16-54-55}$ and $\alpha_{56-57-18-24}$ in all selected solvents for TPP-PPI, and the situation can be amplified by increasing solvent polarity. It proves that the conformation adjustment of acceptor (TPP) in excited states plays important roles on inducing PLICT character.

The assortive evidence appears in bond length. The bond length of L_{22-30} , L_{33-37} , L_{31-32} , and L_{34-35} in ground state of TPP-PPI in *n*-hexane are 1.485, 1.486, 1.333, and 1.332 Å, respectively, which match the common bond length of C_{Ar}-C_{Ar} (1.487 Å) and C_{sp2} = N (1.336 Å) respectively.^[16] However, the L_{22-30} , L_{33-37} , L_{31-32} , and L_{34-35} are shorten to 1.417, 1.455, 1.320, and 1.308 Å in excited state, respectively. This variation indicates the conformation on acceptor unit of TPP-PPI prefers to form quinoid structure owing to its stability in excited state. Combining with the contribution of L_{16-54} and L_{18-57} , the large conjugative plane is formed after excitation as Figure 5B shown. Furthermore, the difference of these selected bond length between ground states and excited states in Table 3,

testifies that the process of TPP unit converting to its quinoid structure furnishes much contribution to the formation of PLICT and the amplifying effect from the non-polar solvent to high polar solvent is confirmed again, similar to the change of dihedral angles. The structures of TPP-PPI in excited states are also flatter than that in ground states whatever the solvent surrounds just as the TPP-PPI (Figure S24 and Table S7, Supporting Information).

Based on the analysis from the calculated and experimental results, the improvement of Φ_s and redshift fluorescence of TPP-based materials do originate from PLICT process in their excited states, and the ESQIP process in excited states might give larger contribution to enforce the PLICT process.

2.4. Electroluminescence

Employing these two compounds with PLICT properties in OLED devices, the non-doped OLEDs devices with the

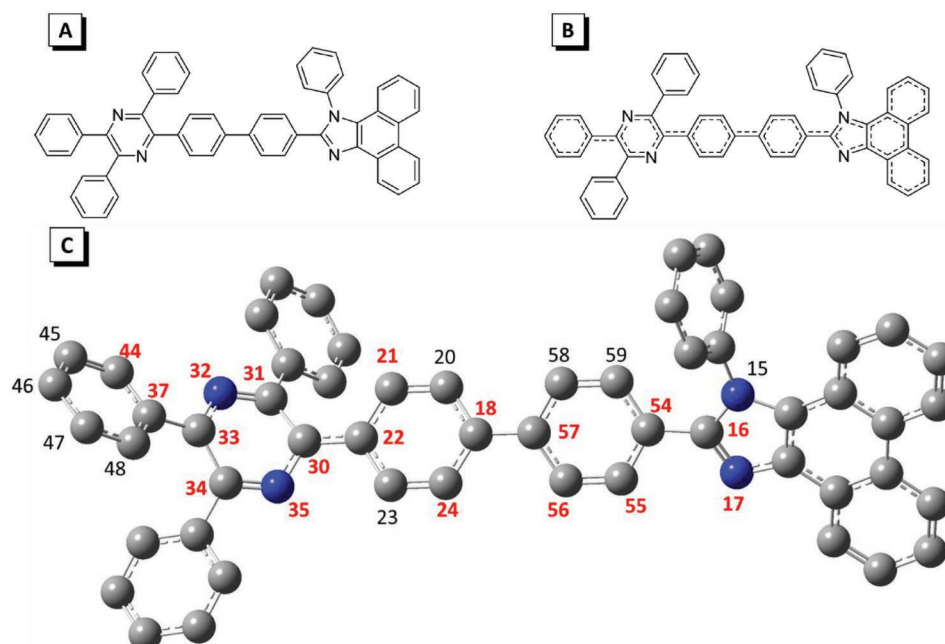


Figure 5. A) The common structure and B) quinoid structure of TPP-PPI; and C) the label atoms on the TPP-PPI.

Table 4. The electroluminescence performance of Devices I and II.

Device	$V_{on}^a)$ [V]	Maximum values				Values at 1000 $cd\ m^{-2}$					
		$\eta_C^b)$ [$cd\ A^{-1}$]	$\eta_p^b)$ [$lm\ W^{-1}$]	EQE ^{b)} [%]	$L^b)$ [$cd\ m^{-2}$]	$\eta_C^b)$ [$cd\ A^{-1}$]	$\eta_p^b)$ [$lm\ W^{-1}$]	EQE ^{b)} [%]	CIE (x,y) ^{c)}	$\lambda_{EL}^d)$ [nm]	Roll-off ^{e)} [%]
I	2.9	8.34	8.18	4.85	16 460	7.76	6.10	4.51	(0.156, 0.232)	474	5.13
II	2.9	8.50	8.23	4.36	16 890	8.04	6.32	4.12	(0.163, 0.285)	484	5.41

Abbreviations: ^{a)} V_{on} = turn-on voltage at 1 $cd\ m^{-2}$; ^{b)} η_C = current efficiency; η_p = power efficiency; EQE = external quantum efficiency; and L = luminance; ^{c)}CIE = Commission International de l'Eclairage coordinates; ^{d)} λ_{EL} = maxima of electroluminescent spectra; ^{e)}EQE roll-off of the max one and the one at 1000 $cd\ m^{-2}$.

configuration of ITO/HATCN (5 nm)/NPB (40 nm)/TcTa (5 nm)/EML (20 nm)/TPBi (40 nm)/LiF (1 nm)/Al were fabricated, where the EML of Device I and Device II are TPP-PPI and TPP-PI, respectively. In the devices, hexaazatriphenylene-hexacarbonitrile (HATCN) and N,N'-Bis(naphthalen-1-yl)-N,N'-bis(phenyl)benzidine (NPB) serve as hole-injecting layer and hole-transporting layer, respectively. 4,4',4''-tri(9-carbazoyl)triphenylamine (TcTa) acts as the hole-transporting and electron-blocking layers, and 2,2',2''-(1,3,5-benzinetriyl) tris(1-phenyl-1-H-benzimidazole) (TPBi) functions as both electron-transporting and hole-blocking layers. The key data and characteristic curves of two devices are given in Table 4 and Figure 6. The two devices are turned on at low voltages of 2.9 V and exhibit stable sky-blue emission with the peaks at 474 and 484 nm, respectively, close to their PL emission in the neat film. These devices both exhibit good EQE with the maximum values of 4.85% and 4.36%, respectively. Under the 1000 $cd\ cm^{-2}$, the EQEs remain to 4.51% and 4.12%, with only about 5% roll-off.

As discussed above, there is a possible reason playing key roles. TPP-PPI and TPP-PI are the PLICT-based materials, whose emission intensity relied on their polar surrounding environment following our mentioned above. The electric field of the devices could construct high polar surrounding for the emitters,^[17] and the Φ_s of the luminescent film would increase with some redshift in electric field, similar to raising the polarity of solvent, so the Φ_s in electroluminescence devices are no longer 28.1% and 20.2%. These expected results suggest that the PLICT process may improve the device performance. Certainly, the detail of every mode contributing to the higher EQE is our important discussion in further work.

3. Conclusion

Following our comprehending of ICT emission, we designed two novel PLICT-typed compounds named as TPP-PPI and TPP-PI. Thanks to the TPP block, whose features are AIE characteristic and stable quinone-conformation in excited state, the new comers exhibit evident AIE and PLICT properties via series of spectral measurements. Combining the analysis from the theoretical calculation in different solvents, their PLICT process and tuning tendency in emission become clear, and the large contribution of the ESQIP is also figured out at the same time. In non-doped OLEDs, these two emitters based on AIE + PLICT process exhibit good performance with high EQE and low roll-off. It implies this novel materials' design strategy that PLICT-based materials with TPP block may achieve high efficiency OLED emitters is feasible and effective. These processes will be confirmed in the further research.

4. Experimental Section

4'-(3,5,6-triphenylpyrazin-2-yl)-[1,1'-biphenyl]-4-carbaldehyde (2): A mixture of intermediate **1** (7 mmol, 3.25 g), 4-formylphenylboronic acid (14 mmol, 2.10 g), $Pd(PPh_3)_4$ (0.35 mmol, 0.40 g), and K_2CO_3 (28 mmol, 3.90 g) was added in 100 mL two-neck bottle under nitrogen. After then, a mixed solvent system of THF and water (v/v = 7:3) 30 mL was injected into the bottle and the mixture was refluxed overnight under nitrogen atmosphere. After cooling to room temperature, the mixture was poured into water and extracted with DCM three times and the combined organic layers were washed with brine, and then dried over $MgSO_4$. The solvent was removed under reduced pressure and the crude product was purified by column chromatography, yield was

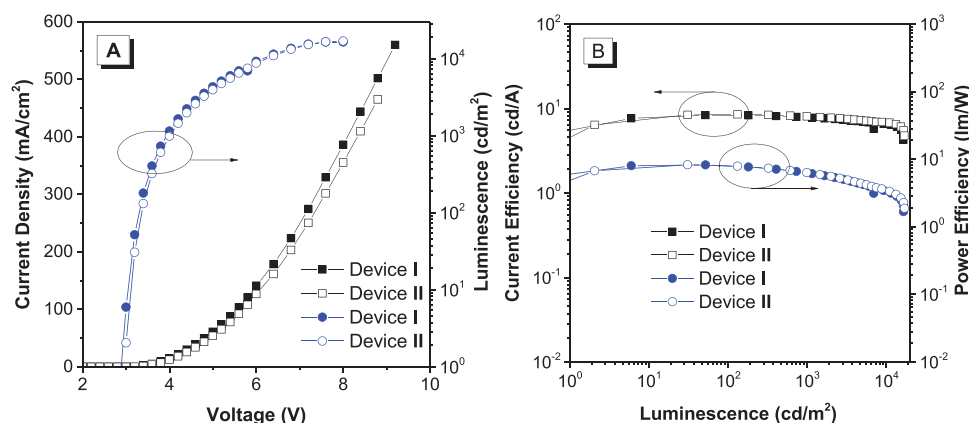


Figure 6. A) Current density–voltage–luminance and B) current efficiency–luminance–power efficiency characteristics of Devices I and II. Device configuration: for Device I, ITO/HATCN (5 nm)/NPB (40 nm)/TcTa (5 nm)/TPP-PPI (20 nm)/TPBi (40 nm)/LiF (1 nm)/Al; and for Device II, ITO/HATCN (5 nm)/NPB (40 nm)/TcTa (5 nm)/TPP-PI(20 nm)/TPBi (40 nm)/LiF (1 nm)/Al.

75%. ^1H NMR (500 MHz, CD_2Cl_2) δ 10.05 (s, 1H), 7.95 (d, J = 8.1 Hz, 2H), 7.81 (d, J = 8.2 Hz, 2H), 7.78–7.72 (m, 2H), 7.70–7.57 (m, 8H), 7.41–7.29 (m, 9H). ^{13}C NMR (126 MHz, CD_2Cl_2) δ 193.01, 150.07, 150.00, 149.97, 149.08, 147.48, 141.02, 140.05, 139.84, 136.85, 131.81, 131.45, 131.17, 131.16, 131.15, 130.06, 129.98, 129.65, 129.53, 128.86, 128.43. HRMS (MALDI-TOF): m/z [M⁺] calculated for $\text{C}_{35}\text{H}_{25}\text{N}_2\text{O}$; 488.1889. found, [M+1] 489.1967.

1-phenyl-2-(4'-(3,5,6-triphenylpyrazin-2-yl)-[1,1'-biphenyl]-4-yl)-1H-phenanthro[9,10-d]imidazole (TPP-PPI): A mixture of **2** (1.5 mmol, 0.73 g), phenanthrenequinone (2.25 mmol, 0.47 g), aniline (7.5 mmol, 0.70 g), ammonium acetate (6 mmol, 0.46 g), and glacial acetic acid (20 mL) were added in 100 mL two-neck bottle and then refluxed under nitrogen for 3 h. After cooling down, the solid product was filtrated and washed with methanol. The crude product was purified by column chromatography, yield is 81%. ^1H NMR (500 MHz, d_6 -DMSO) δ 8.89 (dd, J = 24.3, 8.0 Hz, 1H), 8.73 (d, J = 7.6 Hz, 1H), 7.84–7.47 (m, 11H), 7.37 (s, 5H), 7.07 (d, J = 8.1 Hz, 1H). ^{13}C NMR (126 MHz, CD_2Cl_2) δ 149.96, 149.28, 141.33, 139.94, 139.34, 139.30, 131.82, 131.71, 131.51, 131.49, 131.48, 131.26, 131.16, 130.66, 130.60, 130.41, 130.00, 129.94, 129.63, 129.52, 129.32, 128.81, 127.99, 127.97, 127.81, 127.62, 125.43, 125.11, 124.54, 124.26, 124.19, 122.95, 122.31. HRMS (MALDI-TOF): m/z [M⁺] calculated for $\text{C}_{55}\text{H}_{36}\text{N}_4$; 752.2940. found, [M+1] 753.3013.

1-phenyl-2-(4-(phenylethynyl)phenyl)-1H-phenanthro[9,10-d]imidazole (4): A mixture of intermediate **3** (4 mmol, 1.80 g), CuI (0.08 mmol, 15.2 mg), Pd(PPh₃)₄ (0.04 mmol, 46.2 mg), and was added in 100 mL two-neck bottle under nitrogen. After then, the liquid reactant phenylacetylene, trimethylamine and THF was injected into the bottle and the mixture was refluxed overnight under nitrogen atmosphere. After cooling to room temperature, the solvent was removed under reduced pressure and solid was dissolved into DCM and washed with brine and water, successively. And then, the organic solution was dried over MgSO_4 . The solvent was removed under reduced pressure and the crude product was purified by column chromatography, yield is 85%. ^1H NMR (500 MHz, CD_2Cl_2) δ 8.87–8.70 (m, 3H), 7.79–7.42 (m, 14H), 7.40–7.32 (m, 3H), 7.28 (t, J = 7.5 Hz, 1H), 7.24–7.15 (m, 1H). ^{13}C NMR (126 MHz, CD_2Cl_2) δ 150.18, 138.85, 131.86, 131.65, 131.56, 130.63, 130.36, 129.64, 129.52, 129.49, 129.35, 129.30, 128.84, 128.74, 128.67, 128.57, 127.68, 126.70, 126.03, 125.40, 124.37, 123.50, 123.26, 123.24, 122.89, 121.28, 121.21, 91.17, 89.10. HRMS (MALDI-TOF): m/z [M⁺] calculated for $\text{C}_{35}\text{H}_{22}\text{N}_2$; 470.1783. found, [M+1] 471.1856.

1-phenyl-2-(4-(1-phenyl-1H-phenanthro[9,10-d]imidazol-2-yl)phenyl)ethane-1,2-dione (5): An aqueous solution of KMnO_4 (3 mmol, 1.41 g), NaHCO_3 (3.6 mmol, 0.31 g), and tetraethylammonium bromide (1.5 mmol, 0.21 g) was added into a solution of **4** in DCM. The mixture was rapidly stirred at room temperature for 24 h. The $\text{Na}_2\text{S}_2\text{O}_3$ saturated aqueous solution and 1 M HCl were added into the mixture successively until the solution became clear. The organic layer was separated and washed with brine and water, and dried over MgSO_4 . Evaporation of the solvent afforded nearly pure compound, yield is 93%. ^1H NMR (500 MHz, CD_2Cl_2) δ 8.84–8.80 (m, 1H), 8.78 (d, J = 8.3 Hz, 1H), 8.72 (d, J = 8.3 Hz, 1H), 8.01–7.93 (m, 2H), 7.90–7.85 (m, 2H), 7.79–7.75 (m, 3H), 7.74 (d, J = 1.1 Hz, 1H), 7.73–7.61 (m, 5H), 7.61–7.51 (m, 5H), 7.28 (ddd, J = 8.2, 7.0, 1.1 Hz, 1H), 7.20 (dd, J = 8.3, 0.9 Hz, 1H). ^{13}C NMR (126 MHz, CD_2Cl_2) δ 195.61, 195.15, 149.95, 139.54, 136.34, 134.18, 133.84, 131.87, 131.72, 131.16, 130.89, 130.85, 130.83, 130.37, 130.22, 130.15, 129.76, 128.85, 127.86, 127.38, 126.84, 125.45, 124.56, 124.10, 124.01, 122.44. HRMS (MALDI-TOF): m/z [M⁺] calculated for $\text{C}_{35}\text{H}_{22}\text{N}_2\text{O}_2$; 502.1681. found, [M+1] 503.1759.

1-phenyl-2-(4-(3,5,6-triphenylpyrazin-2-yl)phenyl)-1H-phenanthro[9,10-d]imidazole (TPP-PI): A mixture of **5** (2 mmol, 1.05 g), 1,2-diphenylethane 1,2-diamine (3 mmol, 0.64 g), and glacial acetic acid (20 mL) were added in 100 mL two-neck bottle and then refluxed under air for 3 h. After cooling down, the solid product was filtrated and washed with methanol. The crude product was purified by column chromatography, yield is 65%. ^1H NMR (500 MHz, CD_2Cl_2) δ 8.80 (dd, J = 14.6, 7.6 Hz, 1H), 8.73 (d, J = 8.3 Hz, 1H), 7.81–7.73 (m, 1H), 7.70–7.58 (m, 5H), 7.57–7.50 (m, 3H), 7.40–7.31 (m, 4H), 7.30–7.25 (m, 1H), 7.21 (dd, J = 8.3, 1.0 Hz, 1H). ^{13}C NMR (126 MHz, CD_2Cl_2) δ 150.17, 150.07, 150.03, 149.00, 139.84, 139.82, 139.68, 131.60, 131.36, 131.15,

131.10, 130.95, 130.47, 130.37, 130.05, 129.97, 129.95, 129.62, 129.53, 129.50, 128.73, 127.74, 127.06, 127.03, 126.43, 125.39, 124.94, 124.52, 123.98, 123.31, 122.29. HRMS (MALDI-TOF): m/z [M⁺] calculated for $\text{C}_{49}\text{H}_{32}\text{N}_4$; 676.2627. found, [M+1] 677.2700.

Supporting Information

Supporting Information is available from the Wiley Online Library or from the author.

Acknowledgements

This work is financially supported by National Natural Science Foundation of China (21788102, 51673118, and 51603127), Natural Science Fund of Guangdong Province (2016A030312002), the Innovation and Technology Commission of Hong Kong (ITC-CNERC14SC01), Science and Technology Program of Guangzhou (201804020027, 201804010218, and 201704030069), Science and Technology Plan of Shenzhen (JCYJ20160428150429072 and JCYJ20160229205601482), and the Fundamental Research Funds for the Central Universities (2017JQ013 and 2017B0036).

Conflict of Interest

The authors declare no conflict of interest.

Keywords

aggregation-induced emission, excited state quinone-conformation induced planarization, organic light-emitting diodes, planarized intramolecular charge transfer, tetraphenylpyrazine

Received: February 18, 2019

Revised: April 27, 2019

Published online: June 5, 2019

- [1] a) Q. Zhang, B. Li, S. Huang, H. Nomura, H. Tanaka, C. AdaChi, *Nat. Photonics* **2014**, *8*, 326; b) W. Li, Y. Pan, L. Yao, H. Liu, S. Zhang, C. Wang, F. Shen, P. Lu, B. Yang, Y. Ma, *Adv. Opt. Mater.* **2014**, *2*, 892; c) Z. Wang, Y. Feng, S. Zhang, Y. Gao, Z. Cao, Y. Chen, X. Zhang, P. Lu, B. Yang, P. Chen, Y. Ma, S. Liu, *Phys. Chem. Chem. Phys.* **2014**, *16*, 20772; d) S. Xu, T. Liu, Y. Mu, Y.-F. Wang, Z. Chi, C.-C. Lo, S. Liu, Y. Zhang, A. Lien, J. Xu, *Angew. Chem., Int. Ed.* **2015**, *54*, 874; e) Y. Shi, Y. Cai, Y. J. Wang, M. Chen, H. Nie, W. Qin, H. Zhang, J. Z. Sun, A. Qin, B. Z. Tang, *Sci. China: Chem.* **2017**, *60*, 635; f) J. Yang, L. Li, Y. Yu, Z. Ren, Q. Peng, S. Ye, Q. Li, Z. Li, *Mater. Chem. Front.* **2017**, *1*, 91.
- [2] a) H. Kang, A. Facchetti, H. Jiang, E. Cariati, S. Righetto, R. Ugo, C. Zuccaccia, A. Macchioni, C. L. Stern, Z. Liu, S.-T. Ho, E. C. Brown, M. A. Ratner, T. J. Marks, *J. Am. Chem. Soc.* **2007**, *129*, 3267; b) N. Hebbard, Y. Ramondenc, G. Plé, G. Dupas, N. Plé, *Tetrahedron* **2009**, *65*, 4190; c) S. Yan, R. Huang, Y. Zhou, M. Zhang, M. Deng, X. Wang, X. Weng, X. Zhou, *Chem. Commun.* **2011**, *47*, 1273; d) S. Achelle, A. Barsella, C. Baudequin, B. Caro, F. Guen, *J. Org. Chem.* **2012**, *77*, 4087; e) X. Li, S. Semin, L. A. Estrada, C. Yuan, Y. Duan, J. Cremers, P. Tinnemans, P. Kouwer, A. E. Rowan, T. Rasing, J. Xu, *Chin. Chem. Lett.* **2018**, *29*, 297.

- [3] a) E. Wang, L. Hou, Z. Wang, S. Hellstrom, F. Zhang, O. Inganäs, M. R. Andersson, *Adv. Mater.* **2010**, 22, 5240; b) B. Zhao, C. Yan, Z. Wang, H. Huang, Y. Hu, P. Cheng, M. Yi, C. Huang, X. Zhan, W. Huang, *J. Mater. Chem. C* **2017**, 5, 8988; c) B. He, Q. Yin, X. Yang, L. Liu, X.-F. Jiang, J. Zhang, F. Huang, Y. Cao, *J. Mater. Chem. C* **2017**, 5, 8774; d) P. Cheng, M. Zhang, T. K. Lau, Y. Wu, B. Jia, J. Wang, C. Yan, M. Qin, X. Lu, X. Zhan, *Adv. Mater.* **2017**, 29, 1605216.
- [4] a) T. Hirayama, K. Okuda, H. Nagasawa, *Chem. Sci.* **2013**, 4, 1250; b) W. Cui, L. Wang, G. Xiang, L. Zhou, X. An, D. Cao, *Sens. Actuators, B* **2015**, 207, 281; c) D. Zhou, Y. Wang, J. Jia, W. Yu, B. Qu, X. Li, X. Sun, *Chem. Commun.* **2015**, 51, 10656; d) Y. Chen, Y. Ling, L. Ding, C. Xiang, G. Zhou, *J. Mater. Chem. C* **2016**, 4, 8496; e) M. T. Gabr, F. C. Pigge, *Mater. Chem. Front.* **2017**, 1, 1654; f) Q. Li, Z. Li, *Sci. China: Chem.* **2015**, 58, 1800.
- [5] a) S. Jana, S. Dalapati, N. Guchhait, *J. Phys. Chem. A* **2012**, 116, 10948; b) Y. Wang, Z. He, G. Chen, T. Shan, W. Yuan, P. Lu, Y. Zhang, *Chin. Chem. Lett.* **2017**, 28, 2133; c) Q. Zhang, H. Kuwabara, W. J. Potscavage, S. Huang, Y. Hatae, T. Shibata, C. Adachi, *J. Am. Chem. Soc.* **2014**, 136, 18070.
- [6] S. Sasaki, Y. Niko, A. S. Klymchenko, G. Konishi, *Tetrahedron* **2014**, 70, 7551.
- [7] R. Ghosh, D. K. Palit, *J. Phys. Chem. A* **2015**, 119, 11128.
- [8] O. A. Kucherak, P. Didier, Y. Mély, A. S. Klymchenko, *J. Phys. Chem. Lett.* **2010**, 1, 616.
- [9] a) G. Haberhauer, R. Gleiter, C. Burkhart, *Chem. – Eur. J.* **2016**, 22, 971; b) G. Haberhauer, *Chem. – Eur. J.* **2017**, 23, 9288.
- [10] Z. Zhang, Z. Zhang, Y. Luo, S. Sun, G. Zhang, *Spectrochim. Acta Part A* **2018**, 190, 324.
- [11] a) J. Chen, C. C. W. Lam, J. W. Y. Lam, Y. Dong, S. M. F. Lo, I. D. Williams, D. Zhu, B. Z. Tang, *Chem. Mater.* **2003**, 15, 1535; b) H. Tong, Y. Dong, Y. Hong, M. Häussler, J. W. Y. Lam, H. H. Y. Sung, X. Yu, J. Sun, I. D. Williams, H. S. Kwok, B. Z. Tang, *J. Phys. Chem. C* **2007**, 111, 2287; c) J. He, B. Xu, F. Chen, H. Xia, K. Li, L. Ye, W. Tian, *J. Phys. Chem. C* **2009**, 113, 9892; d) G.-F. Zhang, Z.-Q. Chen, M. P. Aldred, Z. Hu, T. Chen, Z. Huang, X. Meng, M.-Q. Zhu, *Chem. Commun.* **2014**, 50, 12058; e) L. Li, M. Chen, H. Zhang, H. Nie, J. Z. Sun, A. Qin, B. Z. Tang, *Chem. Commun.* **2015**, 51, 4830; f) H. Nie, K. Hu, Y. Cai, Q. Peng, Z. Zhao, R. Hu, J. Chen, S.-J. Su, A. Qin, B. Z. Tang, *Mater. Chem. Front.* **2017**, 1, 1125.
- [12] a) M. Chen, L. Li, H. Nie, J. Tong, L. Yan, B. Xu, J. Z. Sun, W. Tian, Z. Zhao, A. Qin, B. Z. Tang, *Chem. Sci.* **2015**, 6, 1932; b) M. Chen, H. Nie, B. Song, L. Li, J. Z. Sun, A. Qin, B. Z. Tang, *J. Mater. Chem. C* **2016**, 4, 2901; c) L. Pan, Y. Cai, H. Wu, F. Zhou, A. Qin, Z. Wang, B. Z. Tang, *Mater. Chem. Front.* **2018**, 2, 1310; d) L. Pan, H. Wu, J. Liu, W. Luo, P. Chen, Z. Wang, A. Qin, B. Z. Tang, *Adv. Opt. Mater.* **2019**, 7, 1801673.
- [13] S. Zhang, L. Yao, Q. Peng, W. Li, Y. Pan, R. Xiao, Y. Gao, C. Gu, Z. Wang, P. Lu, F. Li, S. Su, B. Yang, Y. Ma, *Adv. Funct. Mater.* **2015**, 25, 1755.
- [14] P. Karastatiris, J. A. Mikroyannidis, I. K. Spiliopoulos, *Macromolecules* **2004**, 37, 7867.
- [15] B. Chen, H. Zhang, W. Luo, H. Nie, R. Hu, A. Qin, Z. Zhao, B. Z. Tang, *J. Mater. Chem. C* **2017**, 5, 960.
- [16] F. H. Allen, O. Kennard, D. G. Watson, L. Brammer, A. G. Orpen, R. Taylor, *J. Chem. Soc., Perkin Trans. 2* **1970**, 12, S1.
- [17] J. Yang, Q. Guo, Z. Ren, X. Gao, Q. Peng, Q. Li, D. Ma, Z. Li, *J. Mater. Chem. C* **2017**, 5, 6185.